

Analysis of a Static Mixer for an Aeronautical Test Bench of the Colombian Air Force: a Numerical Study of the Process Variables

Jose Luis Orellano Lasprilla^a, Camilo Bayona-Roa^a, Mauricio López Gomez^b, Alberth Renne Gonzalez Carantón^{a*}

^aGrupo de Investigación en Aprovechamiento Tecnológico de Materiales y Energía, Universidad ECCI, Bogotá, Colombia

^bGrupo de Investigación en Electrónica y Tecnologías Para la Defensa, TESDA. Escuela de Suboficiales de la Fuerza Aérea Colombiana, ESUFA Fuerza Aérea Colombiana, FAC, Bogotá, Colombia
argonzalezc@ecci.edu.co

Static mixing in conventional fuels is an industrial practice to obtain homogeneous liquid mixtures; due to an obstruction in the flow, the liquid-liquid phase mixtures become homogeneous, since a higher intimate contact is allowed between the mixing substances. This work displays a hydrodynamic simulation of a static mixer using FAME biodiesel and JETA-1 blends with a percentage in volume up to 25% of biodiesel. The main effects on the concentration distribution are obtained as a function of the % of substitution of biofuel and the internal mixer geometry, thus exhibiting different hydrodynamic responses and output properties for the blends. These properties serve as a preliminary reference before achieving experimental measurements in the laboratory.

Keywords: static mixer; JetA-1; Biodiesel, hydrodynamic distribution.

1. Introduction

Mixing of fluids is a relevant industrial operation, especially when it is applied to blending systems in refineries or food and plastic processing. In industrial applications, where a mixed homogeneous system is required to obtain the final product, mixing plays an important role in terms of the quality of the final mixture, energy costs, and turnover of the process. Mixing is carried out in two different ways: one includes a mechanical agitator — known, as dynamic mixers—, and another without the agitator, known, as static mixers (Singh et al., 2009). Static mixers are, thus, efficient devices used for promoting the homogeneous mixing of single and multiphase fluids (Hobbs & Muzzio, 1997). Dynamic mixing (Rauline et al., 2000) is frequently applied when the inlet flow enters in a turbulent regime (Theron & Sauze, 2011). On the other hand, for laminar flow regimes and highly viscous fluids, dynamic mixers require a huge amount of power to mix the fluid which makes them an expensive choice compared to motionless mixers. For viscous fluids in the laminar region, static mixers need less power and perform better than the conventional agitator mixers in terms of mixing operation (Lindenberg et al., 2008). The driven force of static mixers is the kinetic and potential energy of the fluid, based on the momentum of the flowing fluid (Zalc et al., 2002). Additionally, several reductions in costs can be achieved for multiple applications of interest, where cost reduction can be significant. Understanding the physical phenomena of the flow inside the static mixer is a key ingredient in the development of energy reduced technologies involving the mixing of two fluids (Saatdjian et al., 2012). This effort is related to completely describing the separated flow fields generated by the different transport properties of both fluids and the flow patterns between them under the complex conditions of viscous flows (Kumar et al., 2008). Several configurations of static mixers have been proposed, however, the fluid dynamics effects inside this equipment still need to be studied (Berkman & Calabrese, 1988). This is required in order to assure a perfect blend, where the most diluted phase must be distributed homogeneously within the solvent (Rabha et al., 2015). The incompressible Navier-Stokes equations portray a mathematical model that completely describes the two fluid flow. The description made by these equations have the advantage of representing the turbulent Eddies in the continuum limit. However, the main disadvantage is that the analytical solution of those equations is almost impossible for real applications

(Coroneo et al., 2012). Thus, two different approaches can be used instead for representing the turbulent flow inside the static mixer: the first is by means of experimental methods (Theron & Sauze, 2011) whilst the second uses numerical simulations (Hanada et al., 2016). In the present work, the flow description can also be achieved with the second approach: computational simulations, which are inexpensive and fast when used for new designs to predict the system integrity, and calculate real time responses. A finite element variational multiscale formulation is developed to stabilize the numerical solution of the fluid flow problem (Hughes, 1995), particularly, for the spatial approximation, which may suffer from instabilities arising from equal interpolation spaces for unknown velocity and pressure, and convection dominant type of flows. This approach shows accurate and stable numerical descriptions of the two fluid flows modelled by the concentration transport equation, and by including an implicit turbulence modelling in the line of the Implicit Large Eddy Simulation methods in (Bayona et al., 2018). Numerical developments are applied to simulate a static fuel mixer which reduces the risk of saturation present in conventional agitators. This article is organized as follows. In Section 2 we present the static mixer flow setting. Next, in Section 3, we describe the computational methodology used, to numerically simulate the annular flow. Then, in Section 4 we present the numerical results of a complete study of the resulting variables inside the static mixer for different blends. Finally, some concluding aspects about the computational methodology of studying the flow setting are stated in Section 5.

2. Static mixer and operation procedure

2.1 Simplified geometry and operative conditions

The static mixer geometry is presented in Figure 1, as well as the main components of the mixer, which are the pipe, the injection nozzles, and the obstructions. The pipe has a diameter d of 1m and a total length L of 10m. It is considered as a two dimensional flow, with an infinite extension in the depth dimension and the baffles perpendicularly located with respect to the axial direction of the flow. The inlet for the JETA-1 fuel is located at the left wall, where the velocity data is known and prescribed. Two inlets for the biodiesel fuel are located at the upper and lower channel walls and defined from the left-most wall up to a certain horizontal distance b : the Biodiesel is injected in a perpendicular fashion through these inlets in order to represent a jet injection of the solute into the solvent. The first baffle is horizontally separated $l_1 = 2m$ from the inlet. Each baffle has a width of 0.05 m and the axial distance between consecutive baffles is set to be $l_2 = 0.9m$, or exactly $l_3 = 1.8 m$ between baffles at the same side. The turbulent regime load is of main interest, especially the Reynolds 10000 case, for which turbulent effects are relevant in the mixing process. Although turbulence is a three-dimensional process, as commented before, the numerical method has an implicit model of turbulence despite the two dimensional solution. Thus, the JETA-1 velocity at the inlet is fixed at $u = (0.01399)$ m/s. This same speed is set for the biodiesel injection. Nevertheless, the horizontal length b (meaning the transversal area of the injected jet) is modified according to the mass concentration ratio. This study evaluates fuel blends with a percentage in volume up to 25% of biodiesel. In this sense, four different blends are simulated: 5%, 10%, 15% and 25% percentage in volume of biodiesel in JETA-1. The horizontal length b gives 0.026m, 0.055m, 0.088m, and 0.166m, respectively, for these blends and the fixed inlet velocities.

2.2 Mixing Rules

Some mixing rules are used for the description of some mechanical fluid properties of interest, such as: density ρ , kinematic viscosity ν , viscosity μ and Lower Heating Value (LHV). The most important quantity is the mass fraction of each fluid content. In this sense, the mass fraction of JETA-1 is given by the X_J variable, while the mass fraction of FAME biodiesel is X_B for the mixed compound, the fluid properties are given in terms of the mass fractions as,

$$\ln(\rho_M) = X_J \ln(\rho_J) + X_B \ln(\rho_B) \quad (1)$$

$$\ln(\mu_M) = X_J \ln(\mu_J) + X_B \ln(\mu_B) \quad (2)$$

$$\ln(\text{LHV}_M) = X_J \ln(\text{LHV}_J) + X_B \ln(\text{LHV}_B) \quad (3)$$

Where the subscripts J and B refer to the JETA-1 fuel and FAME biodiesel, respectively.

Even though the mixer geometry is not axisymmetric due to the flow obstructions, it is considered as a two dimensional flow only for engineering purposes. This simplification aims to produce a fast output of the mixed bulk properties at the outlet, without resorting to a costly three-dimensional simulation. Also, by assuring the turbulent description of the flow in the two-dimensional framework given by the Implicit Large Eddy Simulation from the Variational Multiscale stabilized finite element formulation (Bayona et al., 2018). Hence, the two-dimensional geometry is considered with an infinite extension in the depth dimension and the baffles perpendicularly located with respect to the axial direction of the flow. The fluid properties for each pure compound are given in Table 1.

Table 1: Pure fluid properties

Property	Units	JETA-1	FAME Biodiesel
Density	kg/m ³	809,49	841,26
Kinematic viscosity	mm ² /s	1.4	4.5
LHV	Pa-s	1.133x10 ⁻³	3.786x10 ⁻³
Density	MJ/kg	42.9	37.08

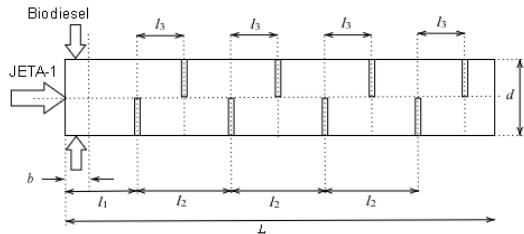


Figure 1: Geometry of static mixer.

2.3 Mass diffusivity relation

The Wilke-Chang equation is used for the diffusivity calculation of liquid biodiesel into liquid JETA-1. This relation is given by $\epsilon_B = C_D \frac{\psi_J M_J T}{\mu_M V_B}$, where $C_D = 7.4 \times 10^{-16} \text{ m}^4/\text{s}^2\text{K}$ is a chemical constant, $\psi_J = 1$ is the molecular association parameter relating the molecular interaction between solvent and solute, $M_J = 0,186 \text{ kg/mol}$ is the molecular weight of JETA-1, $T = 298.15 \text{ K}$ is the flow temperature, and $V_B = 0.05181068 \text{ m}^3/\text{mol}$ is the molar volume of biodiesel (solute) at its normal boiling point.

3. Computational methodology

The Python library dolfin, from the FEniCS Project (Alnæs, M et al., 2015), is used to formulate and numerically solve the problem in variational form. The FEniCS Project provides a novel tool for the automated solution of partial differential equations by the finite element method that we exploit. Next, we present the finite element formulation which is capable of representing the transient two fluid flow.

3.1 Navier-Stokes equations for the fluid flow

The Wilke-Chang equation is used for the diffusivity calculation of liquid biodiesel into liquid JETA-1. In terms of the hydraulic description, the flow velocity and pressure fields are completely described by the incompressible Navier-Stokes equations. These relations are given by

$$\rho_M \partial_t \mathbf{u} + \rho_M (\mathbf{u} \cdot \nabla) \mathbf{u} + \nabla p - 2\mu_M \nabla \cdot (\nabla \mathbf{u}) = \rho_M \mathbf{b}, \quad \forall \mathbf{x} \in \Omega, t \in (0, t_f), \quad (4)$$

$$\nabla \cdot \mathbf{u}, \quad \forall \mathbf{x} \in \Omega, t \in (0, t_f), \quad (5)$$

where $\Omega \subset \mathbb{R}^2$ is the computational domain, and $(0, t_f)$ is the time interval in which the problem is solved. The bulk properties of the mixed flow are calculated using relations (1) - (3). The fluid velocity is $u_i : \Omega_i \times (0, t_f) \rightarrow \mathbb{R}^2$, the pressure is $p : \Omega_i \times (0, t_f) \rightarrow \mathbb{R}$, and the force vector is $\rho_M \mathbf{b} : \Omega \rightarrow \mathbb{R}^2$, which is currently neglected.

3.2 Transport equation for the fluid concentrations

The mixing process is modelled by using a Convection-Diffusion-Reaction transport equation for the fluid concentrations of Biodiesel as a miscible fluid in the JETA-1 flow. Thus, the equation for the biodiesel concentration in the JETA-1 flow is the following:

$$\partial_t \chi_B + \mathbf{u} \cdot \nabla \chi_B - \nabla \cdot (\epsilon_B \nabla \chi_B) = 0, \quad \forall \mathbf{x} \in \Omega, t \in (0, t_f). \quad (6)$$

Complementary, the Jet A-1 mass fraction X_J can be calculated from the total mass relationship $X_J + X_B = 1$. The initial condition of the transport equation is chosen to define the initial concentration ratio between the two fluids. In this sense, a strong Dirichlet boundary condition ζ_G is imposed on the inlet boundaries Γ_G : a separate injection for the FAME biodiesel is set along the pipe radial contour, where $\chi_B = 1$. In the main JETA-1 injection nozzle, this variable is strongly set to $\chi_B = 0$. These strong conditions define the inlet blend ratios for the static mixer setting. The mixing rules, together with the mass and momentum balances that include the mixed properties in the bulk flow, guarantee a complete description of both miscible fluids in the mechanical problem.

3.3 Finite Element approximation of the coupled problem

Let us first recall the space of functions $H(\text{div}, \Omega) \doteq (\mathbf{u} \in (L^2(\Omega))^d \mid \nabla \cdot \mathbf{u} \in L^2(\Omega))$, which is the space where the velocity \mathbf{u} lives $\mathbf{V} \doteq H(\text{div}, \Omega)$. Now, let us denote by $h = \Omega^e$ the finite element partition of the domain Ω , with index e ranging from 1 to the number of elements n_{el} in the finite mesh. The diameter of the element partition is denoted by h . We define the finite test function spaces $\mathbf{V}_h \subset \mathbf{V}$ and $Q_h \subset Q \doteq L^2(\Omega)$ as made of continuous piecewise polynomial functions in space. The Galerkin approximation of the coupled version of (4), (5) and (6) is to find $[\mathbf{u}_h, p_h, \chi_{B,h}] \in \mathbf{V}_h \times Q_h \times Q_h$ such that

$$(\rho_M \partial_t \mathbf{u}_h, \mathbf{v}_h) + (\partial_t \chi_{B,h}, \eta_h) + A([\mathbf{u}_h, p_h, \chi_{B,h}]; [\mathbf{v}_h, q_h, \eta_h]) = L([\mathbf{v}_h, q_h, \eta_h]), \quad \forall [\mathbf{v}_h, q_h, \eta_h] \in \mathbf{V}_h \times Q_h \times Q_h, \quad (7)$$

where (\cdot, \cdot) is the integral of the product of two functions (scalar or vector valued) in the Ω domain. Then the variational forms are defined as:

$$A([\mathbf{u}, p, \chi_B]; [\mathbf{v}, q, \eta]) = a(\mathbf{u}, \mathbf{v}) - b(p, \mathbf{v}) + c(\mathbf{u}; \mathbf{u}, \mathbf{v}) + b(q, \mathbf{u}) + ac(\chi_B, \eta) + cc(\mathbf{u}; \chi_B, \eta), \quad (8)$$

$$L([\mathbf{v}, q, \eta]) = l(\mathbf{v}), \quad (9)$$

$$\text{and: } a(\mathbf{u}, \mathbf{v}) = \mu_M \int_{\Omega} \partial_j u_i \partial_j v_i d\Omega, a_c(\chi_B, \eta) = \epsilon_B \int_{\Omega} \partial_i \eta \partial_i \chi_B d\Omega, b(q, \mathbf{v}) = \int_{\Omega} q \partial_i v_i d\Omega,$$

$$c(\hat{\mathbf{u}}, \mathbf{u}, \mathbf{v}) = \rho_M \int_{\Omega} v_j \hat{v}_i \partial_i u_j d\Omega, c_c(\mathbf{u}; \chi_B, \eta) = \int_{\Omega} \eta u_i \partial_i \chi_B d\Omega, l(\mathbf{v}) = \rho_M \int_{\Omega} f v_i d\Omega \text{ with } \mathbf{u}, \mathbf{v} \in \mathbf{V} \text{ and } p, q, \chi_B, \eta \in Q.$$

In the discrete sense, the problem is to seek the discrete solution $[\mathbf{u}_h, p_h, \chi_{B,h}] \in \mathbf{V}_h \times Q_h \times Q_h$, such that:

$$(\rho_M \partial_t \mathbf{u}_h, \mathbf{v}_h) + (\partial_t \chi_{B,h}, \eta_h) + A([\mathbf{u}_h, p_h, \chi_{B,h}]; [\mathbf{v}_h, q_h, \eta_h]) + A_S(\boldsymbol{\tau}([\mathbf{u}_h, \chi_{B,h}])\mathbf{R}([\mathbf{u}_h, p_h, \chi_{B,h}]); [\mathbf{v}_h, q_h, \eta_h]) = L([\mathbf{v}_h, q_h, \eta_h]), \quad (10)$$

for all $[\mathbf{v}_h, q_h, \eta_h] \in \mathbf{V}_h \times Q_h \times Q_h$. The term $A_S(\boldsymbol{\tau}([\mathbf{u}_h, \chi_{B,h}])\mathbf{R}([\mathbf{u}_h, p_h, \chi_{B,h}]); [\mathbf{v}_h, q_h, \eta_h])$ is a consistent Variational Multi-Scale stabilization term, which is added to overcome the instability problems when the standard Galerkin formulation is applied to the Navier-Stokes problem (Codina & Blasco, 1997). The stabilization term incorporates a matrix of stabilization parameters $\boldsymbol{\tau}([\mathbf{u}_h, \chi_{B,h}])$ that depends on the unknown values, and the residual of the finite element approximation (in vector form) $\mathbf{R}(\cdot)$. We adopt the diagonal definition $\boldsymbol{\tau}([\mathbf{u}_h, \chi_{B,h}]) = \text{diag}(\tau_1(\mathbf{u}_h, \chi_{B,h})\mathbf{I}, \tau_2(\mathbf{u}_h, \chi_{B,h}), \tau_3(\mathbf{u}_h, \chi_{B,h}))$ that was proposed in (Codina & Blasco, 1997), with the 2×2 -identity tensor as \mathbf{I} , and the components of the diagonal matrix of stabilization parameters as $\tau_1^{-1}(\mathbf{u}_h, \chi_{B,h}) = C_1 \mu_M / h^2 + C_2 \rho_M |\mathbf{u}_h| / h$, $\tau_2^{-1}(\mathbf{u}_h, \chi_{B,h}) = C_3 \mu_M + C_4 \rho_M |\mathbf{u}_h| h$, and $\tau_3^{-1}(\mathbf{u}_h, \chi_{B,h}) = C_{1B} / h^2 + C_2 |\mathbf{u}_h| / h$, respectively. The term h is the diameter of the element partition, and $C_1 = 12$, $C_2 = 2$, $C_3 = 1$, and $C_4 = 1$ are numerical parameters. Since the present work is restricted to linear order finite elements, the stabilization variational form is defined as follows:

$$\begin{aligned} A_S(\boldsymbol{\tau}([\mathbf{u}_h, \chi_{B,h}])\mathbf{R}([\mathbf{u}_h, p_h, \chi_{B,h}]); [\mathbf{v}_h, q_h, \eta_h]) \\ \doteq \tau_1(-\rho_M \mathbf{u}_h \cdot \nabla \mathbf{v}_h - \nabla q_h, \rho_M \partial_t \mathbf{u}_h - \rho_M \mathbf{u}_h \cdot \nabla \mathbf{u}_h - \nabla p_h) + \tau_2(-\nabla \cdot \mathbf{v}_h, -\nabla \cdot \mathbf{u}_h) \\ + \tau_3(-\mathbf{u}_h \cdot \nabla \eta_h, \partial_t \chi_{B,h} - \mathbf{u}_h \cdot \nabla \chi_{B,h}). \end{aligned} \quad (11)$$

In the case of the first-order temporal derivative of the fluid flow problem (4) and (6), the second order Backward Differentiation Formula (BDF) scheme is used. The Newton method as the linearization scheme for solving the non-linear coupling at each time step.

4. Results

A finite element mesh composed of 150463 linear triangular elements and 76394 total nodes is used to solve the discrete fluid flow problem. According to the time-averaged numerical results, which are presented in figures 2-5, the following observations are stated. Regarding the flow field, some variations on the velocity and pressure profiles for values up to 25% of biodiesel in the blend are displayed in Figure 2(a). These variations are visible when contrasting the lower (top) and higher (bottom) concentrations of biodiesel in the blends. According to the time-averaged results, the edge effects of flow patterns can be considered as important before the obstructions. A maximum magnitude of the fluid velocity appeared in the regions where the fluid gets in contact with the obstruction, thus validating the efficiency of the static mixer operation, as shown in Figure 2(a).

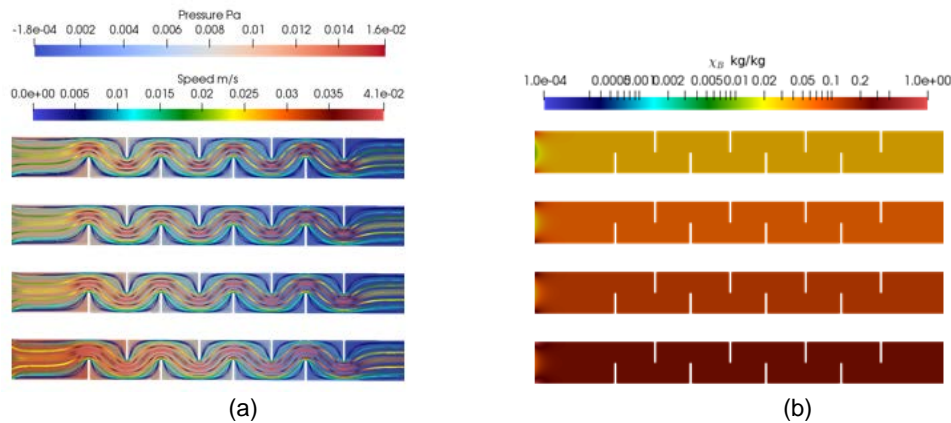


Figure 2: Time-averaged flow field results for the 5%, 10%, 15%, and 25% blends: (a) flow field (b) mass diffusion.

The increased fluid velocity can be considered as a significant consequence of the convective processes in the flow. The present approach, in which different concentrations and several obstructions in the flow are implemented, guarantees a perfect mixing produced by the convective effects. Indeed, these effects are tightly associated with mass, heat, and momentum transfer. The fluid flow results show that for the inlet region of the tube, large gradients occur in a finite and small region near to the perpendicular injection zone where the fluids are in contact. It can be observed that diffusion occurs right from the start of this mixing process. However, Figure 2(b) evidences that the expected theoretical mixing between FAME biodiesel and JETA-1 is not achieved with the geometric configuration used for the computational simulation. This deficiency in the mixing becomes more evident as the percentage of FAME biodiesel increases in the mixture. In consequence, the geometric configuration needs to be improved in terms of speed profile changes and moment transfer. Density profiles along the tube demonstrate that the predominant value is given by the JETA-1 major compound in the mixture. In the case of the 25% of biodiesel injection, significant changes were demonstrated by the results. A maximum value of mass density of 815 Kg/m^3 is evidenced in the mixture. These results are obtained, despite the fact that Figure 3 (a) and (b) validate the mathematical model used to carry out the computational simulations obtaining physically-accurate results. However, for the estimation of the mass density, a correlation of mixture with shrinkage loss parameters could be used along with the fluid flow. This may enable a complete fluid flow visualization of mass density during the convective phenomena and the main effect of obstruction in the mixing process.

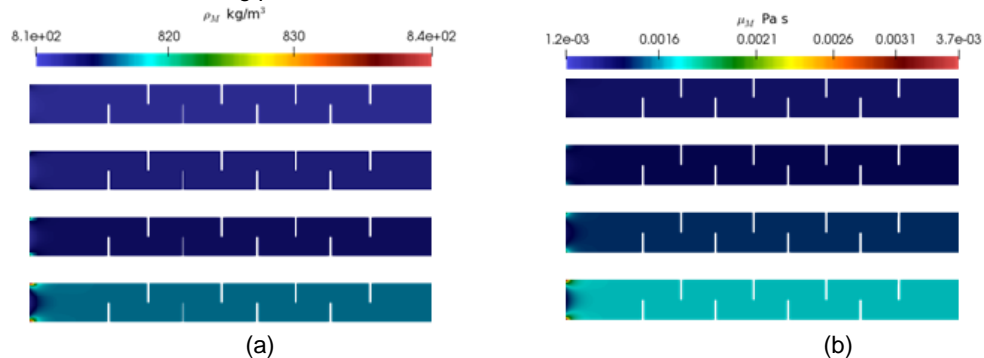


Figure 3: Time-averaged density (a) and viscosity (b) results for the 5%, 10%, 15%, and 25% blends.

The viscosity of the blend demonstrates more significant gradients: for values up to 25% of biodiesel, it exhibits viscosity gradients near to the region of injection of FAME biodiesel. Since the proposed model assumes that the tube is initially filled with the majority compound JETA-1, it is not possible to notice a shrinkage or a deformation effect of one fluid into the other. In the corners of the tube, large viscosity gradients can be appreciated, however, the viscosity profile is homogeneous without significant effects of baffles and with maximum values of $0,0018 \text{ Pa}\cdot\text{s}$ for dynamic viscosity in the axial length. For each of the FAME biodiesel and JETA-1 blends evaluated, the decrease in the Lower Heating Calorific value is minimal. This variable is

considered of great relevance in this type of analysis, because it allows determining the energetic parameters of the aviation test bench. The results are concordant with experimental measurements made over JETA-1/Biodiesel blends with the same blending proportions, exhibiting values between 41 and 43 MJ/Kg.

5. Conclusions

Some highlights in the mixing process of a static mixer have been observed when numerically solving two-fluid dynamics models given by the Navier-Stokes equations for incompressible fluids. The developed numerical strategy enables computational fluid dynamic results, which showed spatial gradients in the convective phenomena of biodiesel mixing in JETA-1 fuel. Velocity gradients can be associated with the effect of baffles over the natural path of both mixed phases, however, the computational model exhibited no significant distortions and contractions of both mixing fluids, nor the consequences of this phenomena over transport properties, like mass density and dynamic viscosity. This can be explained by the mass correlation that have been used for these properties in the physical and mixing model.

Acknowledgments

This research was financed by COLCIENCIAS with resources from the autonomous patrimony National Fund of Financing for Science, Technology and Innovation Francisco José de Caldas, within the framework of the project entitled "Evaluation of the behaviour of Colombian biofuel mixtures in aeronautical turbines". The authors also acknowledge the Colombian Air Force and ECCI University support.

References

- Alnæs, M. S., Blechta, J., Hake, J., Johansson, A., Kehlet, B., Logg, A., Richardson, C., Ring, J., Rognes, M. E., Garth N. Wells., 2015, The FEniCS Project Version 1.5. *The FEniCS Project Version 1.5*, 3(100), 9–23.
- Bayona, C., Baiges, J., Codina, R., 2018, Variational multiscale approximation of the one-dimensional forced Burgers equation: The role of orthogonal subgrid scales in turbulence modeling. *International Journal for Numerical Methods in Fluids*, 86(5), 313–328.
- Berkman, P. D., Calabrese, R. V., 1988, Dispersion of viscous liquids by turbulent flow in a static mixer. *AIChE Journal*, 34(4), 602–609.
- Codina, R., Blasco, J., 1997, A finite element formulation for the Stokes problem allowing equal velocity-pressure interpolation. *Computer Methods in Applied Mechanics and Engineering*, 143(3–4), 373–391.
- Coroneo, M., Montante, G., Paglianti, A., 2012, Computational fluid dynamics modeling of corrugated static mixers for turbulent applications. *Industrial and Engineering Chemistry Research*, 51(49), 15986–15996.
- Hanada, T., Kuroda, K., Takahashi, K., 2016, CFD geometrical optimization to improve mixing performance of axial mixer. *Chemical Engineering Science*, 144, 144–152.
- Hobbs, D. M., Muzzio, F. J., 1997, The Kenics static mixer: A three-dimensional chaotic flow. *Chemical Engineering Journal*, 67(3), 153–166.
- Hughes, T. J. R., 1995, Multiscale phenomena: Green's functions, the Dirichlet-to-Neumann formulation, subgrid scale models, bubbles and the origins of stabilized methods. *Computer Methods in Applied Mechanics and Engineering*, 127(1–4), 387–401.
- Kumar, V., Shirke, V., Nigam, K. D. P., 2008, Performance of Kenics static mixer over a wide range of Reynolds number. *Chemical Engineering Journal*, 139(2), 284–295.
- Lindenberg, C., Schöll, J., Vicum, L., Mazzotti, M., Brozio, J., 2008, Experimental characterization and multi-scale modeling of mixing in static mixers. *Chemical Engineering Science*, 63(16), 4135–4149.
- Rabha, S., Schubert, M., Grugel, F., Banowski, M., Hampel, U., 2015, Visualization and quantitative analysis of dispersive mixing by a helical static mixer in upward co-current gas-liquid flow. *Chemical Engineering Journal*, 262, 527–540.
- Rauline, D., Le Blévec, J.-M., Bousquet, J., Tanguy, P. A., 2000, A Comparative Assessment of the Performance of the Kenics and SMX Static Mixers. *Chemical Engineering Research and Design*, 78(3), 389–396.
- Saadatian, E., Rodrigo, A. J. S., Mota, J. P. B., 2012, On chaotic advection in a static mixer. *Chemical Engineering Journal*, 187, 289–298.
- Singh, M. K., Anderson, P. D., Meijer, H. E. H., 2009, Understanding and Optimizing the SMX Static Mixer. *Macromolecular Rapid Communications*, 30(4–5), 362–376.
- Theron, F., Sauze, N. Le., 2011, Comparison between three static mixers for emulsification in turbulent flow. *International Journal of Multiphase Flow*, 37(5), 488–500.
- Zalc, J. M., Szalai, E. S., Muzzio, F. J., Jaffer, S., 2002, Characterization of flow and mixing in an SMX static mixer. *AIChE Journal*, 48(3), 427–436.